Journal of Applied Polymer Science

Thiophene π-bridge effect on photovoltaic performances of dithienosilole and bithiazole backboned polymers

Huilin Zheng,[1,2*] Chuantao Gu,[2,3*] Qianqian Zhu,[4] Xichang Bao,[2] Shuguang Wen,[2] Meng Qiu,[2] Dangqiang Zhu,[2,3] Mingliang Sun,[1] Renqiang Yang[2]

[1]Institute of Materials Science and Engineering, Ocean University of China, Qingdao, Shandong 266100, China
[2]CAS Key Laboratory of Bio-based Materials, Qingdao Institute of Bioenergy and Bioprocess Technology, Chinese Academy of Sciences, Qingdao 266101, China
[3]University of Chinese Academy of Sciences, Beijing 100049, China
[4]College of Materials Science and Engineering, Qingdao University of Science and Technology, Qingdao 266042, China
*These authors contributed equally to this work.
Correspondence to: M. Sun (E-mail: mlsun@ouc.edu.cn) and R. Yang (E-mail: yangrq@qibebt.ac.cn)

ABSTRACT: In this article, two dithienosilole (DTS) and bithiazole (BTz) backboned donor–acceptor (D-A) copolymers with (poly{5-(5-(4,4-bis(2-ethylhexyl)-4H-silolo[3,2-b:4,5-b']dithiophen-2-yl)thiophen-2-yl)-4,4'-dinonyl-5'-(thiophen-2-yl)-2,2'-bithiazole} (PDTS-DTBTz)) and without (poly{5-(4,4-bis(2-ethylhexyl)-4H-silolo[3,2-b:4,5-b']dithiophen-2-yl)-4,4'-dinonyl-2,2'-bithiazole} (PDTS-BTz)) thiophene π-bridge were synthesized to study the influence of thiophene π-bridge on their photovoltaic performances. Both polymers show similar band gap, but polymer with thiophene π-bridge (PDTS-DTBTz) has a higher molecular weight, narrower polydispersity index (PDI), more planar geometry, higher crystallinity, higher hole mobility, and better miscibility with fullerene (polymer solar cells (PSCs) acceptor). Although PDTS-BTz polymer based PSCs devices show higher open circuit voltage (V_{oc}), PDTS-DTBTz polymer does show higher power conversion efficiency (PCE) with improved short circuit current density (J_{sc}) and fill factor (FF). The present results indicate that thiophene π-bridge does contribute to the PSCs performances of dithienosilole and bithiazole backboned copolymer. © 2015 Wiley Periodicals, Inc. J. Appl. Polym. Sci. **2015**, *132*, 42798.

KEYWORDS: morphology; optical and photovoltaic applications; optical properties; X-ray

Received 12 June 2015; accepted 30 July 2015
DOI: 10.1002/app.42798

INTRODUCTION

Recently, polymer solar cells (PSCs) have been intensively studied for their flexibility, lightweight, easy fabrication, moderate cost, etc.[1–5] The bicontinuous interpenetrating bulk heterojunction (BHJ) PSCs based on conjugated polymer donor and fullerene (such as $PC_{61}BM$ and $PC_{71}BM$) acceptors have achieved high power conversion efficiency (PCE) exceeding 10%.[6–8] Great efforts have been dedicated to synthesizing narrow band gap polymer to harvest more solar energy,[9–11] and one of the most successful strategy to realize low band gap is alternating different electron-rich (D-donor) and electron-deficient (A-acceptor) units in the polymer backbone (D-A polymer).[12] Besides donor and acceptor units, there are also some π-bridge (conjugated unit, typically thiophene or alkylthiphene units) in the polymer structure (D-π-A polymer)[13–17] Such as, in 2003, Andersson and coworkers introduced thiophene π-bridge into fluorene and benzothiadizole (BT) backboned polymer,[18] and the *PCE* of this material based PSCs can be improved significantly due to the extended light absorption. This has been proven to be an effective way due to the weak electron donating capability of the fluorene segment in the polymer backbone.

In order to further improve the *PCE* of PSCs, various kinds of donor and acceptor were extensively explored. Among them, dithienosilole (DTS) donor based polymers became popular because of their rigid coplanar structure with stronger π–π intermolecular interactions, high photochemical stability, and strong electron-donating properties.[19–24] The DTS-based polymers have been studied by several groups, a high 7.3% PCE is achieved by Ye Tao and coworkers which shows that the DTS-based polymer is one of the high performances PSCs donor materials.[22] Just as the other kind of D-A polymer, DTS was copolymerized with typically acceptor benzothiadizole, and this

Additional Supporting Information may be found in the online version of this article.

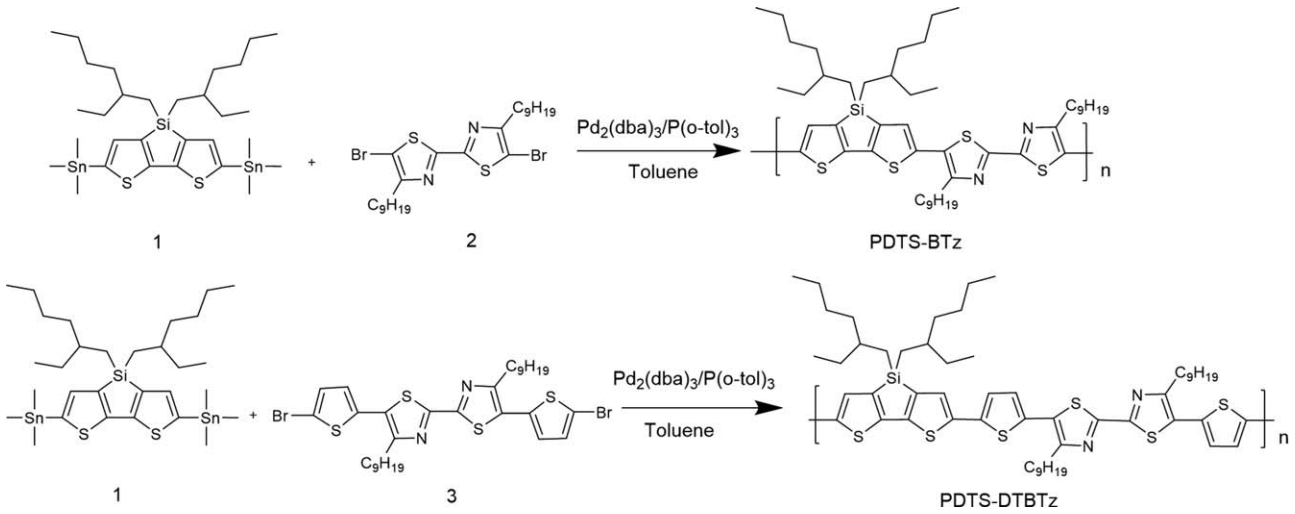

Scheme 1. Synthetic route and chemical structure of PDTS-BTz and PDTS-DTBTz.

materials show high performances with ca. 5% PCE.[19] In contrast to fluorene and BT backboned polymer, inserting π-bridge (thiophene) in the DTS-BT backboned polymer could not improve the PSCs performance.[20] While for benzotriazole (BTA, a relatively weak electron acceptor compared with BT), inserting π-bridge (thiophene) in the DTS-BTA backboned polymer does contribute to the PSCs performances.[25]

Bithiazole (BTz) is reported as a weak acceptor which contains the electron-withdrawing nitrogen of imine (C═N) in place of carbon atom at the 2 and 2'-position of bithiophene.[12] In recent years, Li and Chu and their coworkers have been focused on DTS donor and BTz acceptor backboned polymer (DTS-BTz).[26–31] These polymers bridged by different heteroaromatic rings showed moderate PCE between 2.86% and 3.82%.

In this article, we synthesized two DTS and BTz backboned polymers (shown in Scheme 1), and investigated the effect of thiophene π-bridge on photovoltaic performance. N-nonyl and 2-ethylhexyl were used as side chains to improve the polymer solubility. The present results suggest that, the thiophene π-bridge does contribute to the high quality DTS-BTz photovoltaic polymer (including molecular weight, crystallinity, carrier mobility, and miscibility with fullerene, etc.)

EXPERIMENTAL

Materials

All chemicals and solvents were purchased from commercial sources and used as received unless otherwise noted, and water sensitive reactions were performed under a nitrogen atmosphere. Tetrahydrofuran (THF) and toluene were distilled before use.

Synthesis of PDTS-BTz and PDTS-DTBTz

Both polymers were prepared by the coupling reaction between DTS and DTBTz or BTz. In a 25 mL round-bottom flask, DTS, BTz (or DTBTz), tri(dibenzylideneacetone)dipalladium (6 mg), and tri(o-tolyl)phosphine (14 mg) were subjected to three cycles of evacuation/nitrogen purging and then 6 mL of anhydrous toluene was added. The mixture was heated to 110°C carefully, and the reactant was then stirred for 36 h under a nitrogen atmosphere. The reaction mixture was cooled down to room temperature and precipitated in methanol. The precipitate was filtered and then purified by Soxhlet extraction with methanol, hexane, and $CHCl_3$ in succession. $CHCl_3$ fractions were collected, concentrated, reprecipitated in methanol again, and dried under vacuum overnight to get the target polymers.

PDTS-BTz: DTS (144.8 mg, 0.1946 mmol) and BTz (112.6 mg, 0.1946 mmol) were used, and the polymer was obtained as a blue solid (104 mg, yield 64%). ^{1}H nuclear magnetic resonance (NMR) (600 MHz, $CDCl_3$): δ (ppm) 7.16 (br, 2H), 2.98 (br, 4H), 1.82 (br, 4H), 1.28 (br, 46H), 0.84 (br, 18H).

PDTS-DTBTz: DTS (142.7 mg, 0.1917 mmol) and DTBTz (142.4 mg, 0.1917 mmol) were used, and the polymer was obtained as a dark blue solid (165 mg, yield 85%). ^{1}H NMR (600 MHz, $CDCl_3$): δ (ppm) 7.16 (br, 2H), 7.10 (br, 4H), 2.98 (br, 4H), 1.82 (br, 4H), 1.30 (br, 46H), 0.87 (br, 18H).

Measurement

^{1}H NMR spectra were recorded using a Bruker Advance III 600 (600 MHz) spectrometer in $CDCl_3$ and ambient conditions. The molecular weight of the polymer was measured by Gel permeation chromatography (GPC), and polystyrene was used as a standard with THF as the eluent. Thermogravimetric analysis (TGA) measurements were performed by a STA-409 at a heating rate of 10°C min^{-1} under nitrogen atmosphere. UV–vis absorption spectra were recorded using a Hitachi U-4100 spectrophotometer. Cyclic voltammetry (CV) was performed on a CHI 660D electrochemical workstation with a three-electrode system consisting of a platinum disk working electrode (2.0 mm in diameter), a saturated calomel reference electrode (SCE), and a platinum wire counter electrode in a solution of 0.1 *M* tetrabutylammonium phosphorus hexafluoride (Bu_4NPF_6) in acetonitrile at a scan rate of 50 mV s^{-1}. Polymer thin films were coated from chloroform solution onto the platinum working electrodes and dried under nitrogen before measurement. The redox potential of the ferrocene/ferrocenium (Fc/Fc^+) internal reference is 0.39 V vs. SCE. X-ray diffraction (XRD) spectra were recorded on a Bruker D8

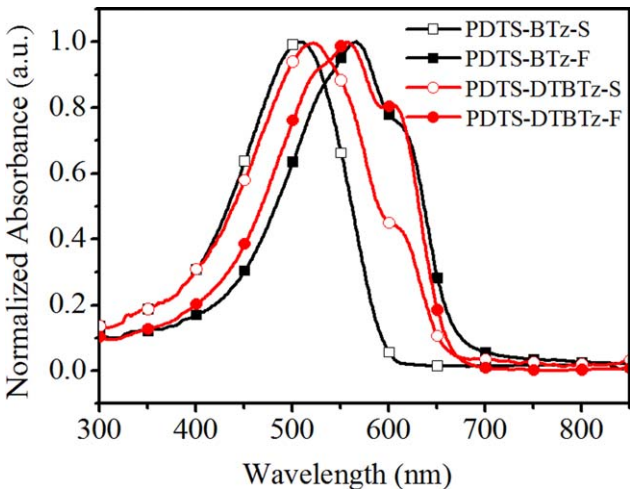

Figure 1. UV–Vis absorption spectra of PDTS-BTz and PDTS-DTBTz in dilute $CHCl_3$ solution and in thin film. [Color figure can be viewed in the online issue, which is available at wileyonlinelibrary.com.]

Advance Spectra. Surface roughness and morphology of the thin films were characterized by atomic force microscopy (AFM) on an Agilent 5400.

Device Fabrication

Photovoltaic devices were fabricated with indium tin oxide (ITO) glass (15 mm × 15 mm) as an anode and a layered structure of ITO/PEDOT:PSS (40 nm)/polymer:$PC_{71}BM$ blend (~110 nm)/Ca (10 nm)/Al (100 nm). The ITO-coated glass substrates were cleaned in an ultrasonic bath in acetone, methanol, and isopropyl alcohol sequentially. The substrates were treated by oxygen plasma for 6 min, then spin-coated with PEDOT:PSS at 4000 rpm, and annealed in an oven for 20 min at 160°C. The polymer and $PC_{71}BM$ were dissolved in deoxygenated anhydrous dichlorobenzene (DCB) or chlorobenzene (CB) in the weight ratios 3 : 2, 1 : 1, 1 : 2, and 1 : 3 and the total concentration of the polymer/$PC_{71}BM$ blending solution was 25 mg mL^{-1}. The solutions were stirred overnight in a nitrogen filled glove box. An active layer consisting of the blend of the polymer and $PC_{71}BM$ was then spin coated on PEDOT:PSS. Subsequently, Ca (10 nm) and Al (100 nm) were thermally evaporated at a vacuum of ~2×10^{-4} Pa on top of the active layer as a cathode. The cathode area defines the active area of the devices, which is 0.1 cm^2. The photovoltaic performance was characterized under illumination with an AM 1.5 G (100 mW cm^{-2}), and current density vs. voltage (*J–V*) curves were recorded by Keithley 2420. External quantum efficiencies of solar cells were analyzed by a certified Newport incident photon conversion efficiency (IPCE) measurement system.

RESULTS AND DISCUSSION

Synthesis and Characterization of the Polymers

The monomers are synthesized according to Supporting Information Scheme S1. PDTS-BTz and PDTS-DTBTz polymer (Scheme 1) were prepared by Stille coupling polymerization in good yields (64%–85%), using a $Pd_2(dba)_3/P(o\text{-}tol)_3$ catalytic. BTz and DTBTz were synthesized according to reported methods.[31] The structures of monomers and polymers were determined by ^{1}HNMR spectroscopy (Supporting Information Figures S1–S5). Both polymers show excellent solubility in common organic solvents, such as chloroform, chlorobenzene (CB), and o-dichlorobenzene (o-DCB). The number average molecular weights (M_n) and weight average molecular weight (M_w) of PDTS-BTz and PDTS-DTBTz were found to be 8.83/15.79 (M_n/M_w) and 44.10/56.76 kg mol^{-1} with polydispersity index (PDI) of 1.8 and 1.3, respectively. The GPC data showed that the thiophene π-bridge help the polymer to achieve high molecular weight and narrow polydispersity index. Thermal stability of the polymers was investigated by TGA. The thermal decomposition temperature (5% weight-loss under nitrogen atmosphere) of PDTS-BTz and PDTS-DTBTz were 440°C and 435°C, respectively. The thiophene π-bridge seems rarely affect the thermal stability of the polymers.

Optical Properties

The UV–vis absorption spectra of PDTS-BTz and PDTS-DTBTz in dilute chloroform solutions and in thin films were shown in Figure 1, and the detailed data are summarized in Table I. The absorption spectra of both polymer films show red-shift in comparison with that of their solutions, owing to the conjugated polymer main chains aggregation in thin film. The red-shift of PDTS-BTz is stronger than PDTS-DTBTz, indicating high aggregation tendency in film state (consistent with the AFM images part). Shoulder peaks can be observed in both solution and film of PDTS-DTBTz at around 609 nm

Table I. Optical and Electrochemical Properties

	UV–vis absorption spectra				Cyclic voltammetry	
	Solution[a]	Thin film[b]				
Polymers	λ_{max} (nm)	λ_{max} (nm)	λ_{onset} (nm)	E_g^{opt} (eV)[c]	E_{on}^{ox}/HOMO (V/eV)	LUMO (eV)[d]
PDTS-BTz	507	566	670	1.85	0.94/-5.35	−3.50
PDTS-DTBTz	521	555	662	1.87	0.71/-5.12	−3.25

[a] Measured in $CHCl_3$ solution.
[b] Cast from $CHCl_3$solution.
[c] Band gap estimated from the UV–vis onset wavelength (λ_{onset}): $E_g^{opt} = 1240/\lambda_{onset}$.
[d] Calculated from LUMO = E_g^{opt} + HOMO.

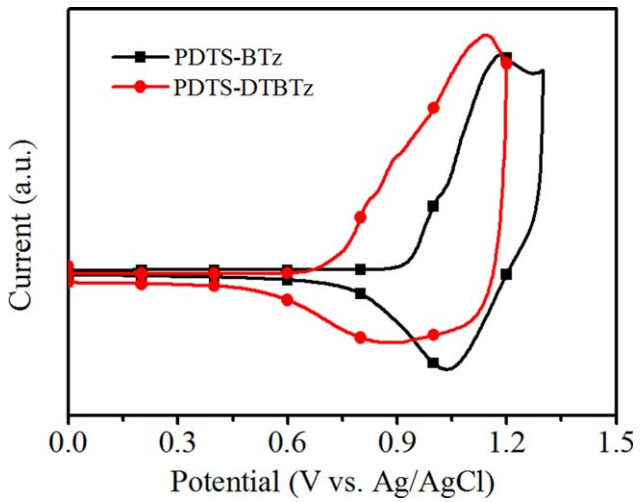

Figure 2. Cyclic voltammograms of PDTS-BTz and PDTS-DTBTz. [Color figure can be viewed in the online issue, which is available at wileyonlinelibrary.com.]

and the film of PDTS-BTz at around 612 nm, these peaks should be attributed to intermolecular π–π^* transitions due to the aggregations of the polymer backbone.[32] The shoulder peaks of PDTS-DTBTz are closely in solution and film, which means a good π–π stacking even in solution state. The absorption onset (λ_{onset}) of PDTS-BTz and PDTS-DTBTz films are 670 and 662 nm, with an optical band gap (E_g^{opt}) of 1.85 and 1.87 eV, respectively. The slight difference of the E_g^{opt} of PDTS-BTz and PDTS-DTBTz is in agreement with previously reported results,[21] which indicates that introducing π-bridge to the DTS-BTz backboned polymer does not affect the E_g^{opt} obviously.

Electrochemical Properties

Cyclic voltammetry of PDTS-BTz and PDTS-DTBTz thin films was performed. The energy level of saturated calomel reference electrode (SCE) was calibrated against the Fc/Fc^+ system to be 4.41 eV in this work. As shown in Figure 2, PDTS-BTz and PDTS-DTBTz showed oxidation onset at 0.94 and 0.71 V, respectively, corresponding to highest-occupied molecular orbital (HOMO) levels of −5.35 and −5.12 eV, respectively. The polymer without thiophene bridge showed relatively low HOMO level, thus a higher value of V_{oc} for PSCs based on PDTS-BTz:$PC_{71}BM$ could be expected, since V_{oc} is related to the offset between the HOMO of polymer donor and the lowest unoccupied molecular orbital (LUMO) of the fullerene acceptor.[16] The LUMO levels of PDTS-BTz and PDTS-DTBTz were determined to be approximately −3.50 and −3.25 eV by using its HOMO energy level and the E_g^{opt}. The calculated LUMO levels of PDTS-BTz and PDTS-DTBTz are 0.6 and 0.85 eV above the LUMO level (−4.1 eV) of $PC_{71}BM$, respectively, which can provide enough driving force for the separation of photo-generated exciton in the PSCs D-A interfaces.

Theoretical Calculation

To understand thiophene π-bridge effect on molecular architecture and optoelectronic properties, molecular stimulation was carried out by using density functional theory (DFT) calculation. To simplify the calculation, all the alky side chains were replaced by methyl groups, and only one repeating unit of each polymer was calculated. The optimized geometry, the stimulated electron density distributions along with the calculated HOMO and LUMO levels are shown in Figure 3. It can be found that the dihedral angle between the DTS and BTz units is smaller in PDTS-DTBTz, which is owing to the reduced steric hindrance by the insertion of thiophene as a bridge. Although all of the dihedral angles are relatively small, much bigger angles and

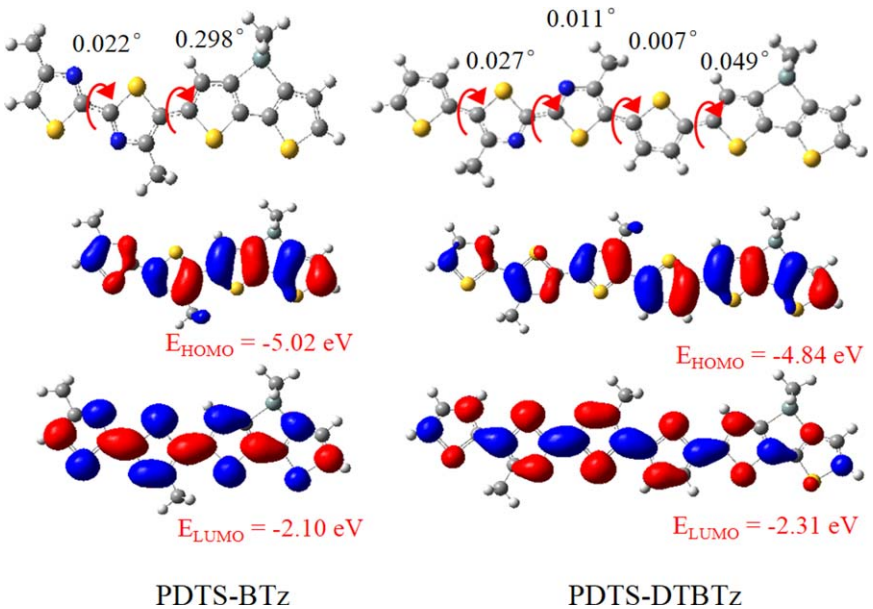

Figure 3. Optimized molecular geometries and frontier molecular orbitals from DFT calculations on PDTS-BTz and PDTS-DTBTz with a simplified chain at the B3LYP/6-31G(d) level of theory. [Color figure can be viewed in the online issue, which is available at wileyonlinelibrary.com.]

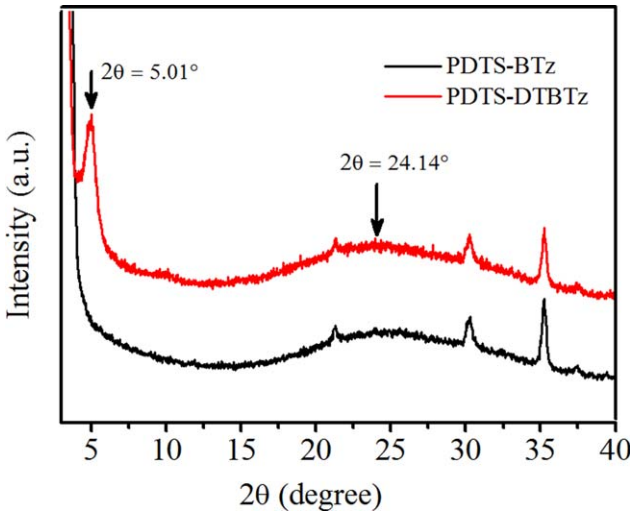

Figure 4. X-ray diffraction patterns of PDTS-BTz and PDTS-DTBTz films. [Color figure can be viewed in the online issue, which is available at wileyonlinelibrary.com.]

significant difference between PDT-BTz and PDTS-DTBTz can be inferred in actual polymer structures. The electron density is well delocalized along the conjugated backbone of both polymers, though a slightly biased toward the DTS unit is found in PDTS-BTz polymer, which can result in a slightly lower HOMO level of PDTS-BTz. The calculated HOMO levels tendency is consistent to the experimental results.

X-ray Diffraction

XRD analysis of PDTS-BTz and PDTS-DTBTz films on ITO substrates (the peaks in the angle of 21°, 30°, and 35° refer to ITO substrate) provided polymer ordering and packing information. As Figure 4 shows, there is a sharp peak in the XRD pattern of PDTS-DTBTz at small angle of $2\theta = 5.01°$, implying that PDTS-DTBTz film featured ordered edge-on nonyl side chains.[33] Substitution of the angle value into the Bragg equation yields a mean interlayer spacing of 17.6 Å for PDTS-DTBTz film, which is ca. 0.2 Å larger than similar polymer reported,[31] and it is probably caused by the longer substituent alkyl group. However, there is no small angle peak in PDTS-BTz XRD pattern, suggesting low crystallinity of PDTS-BTz, which is probably due to the space steric hindrance resulted from long side chain of PDTS-BTz polymer without a thiophene π-bridge. It is reported that edge-on packing improves the hole mobility,[34] and a higher hole mobility of PDTS-DTBTz can be expected. Both polymers show a broad peak at around $2\theta = 24°$, the broad low XRD peak indicates that the π–π stacking in the polymers occurs only in very small regions and the copolymers mainly show amorphous structure.

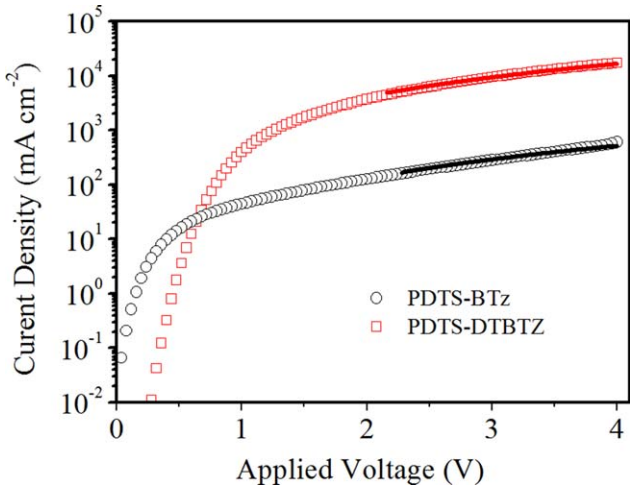

Figure 5. The *J-V* curves of the ITO/PEDO:PSS/Polymer:$PC_{71}BM$/Au diodes. The symbols are experimental data for the transport of holes, and the solid lines are fitted according to the space-charge-limited-current model. [Color figure can be viewed in the online issue, which is available at wileyonlinelibrary.com.]

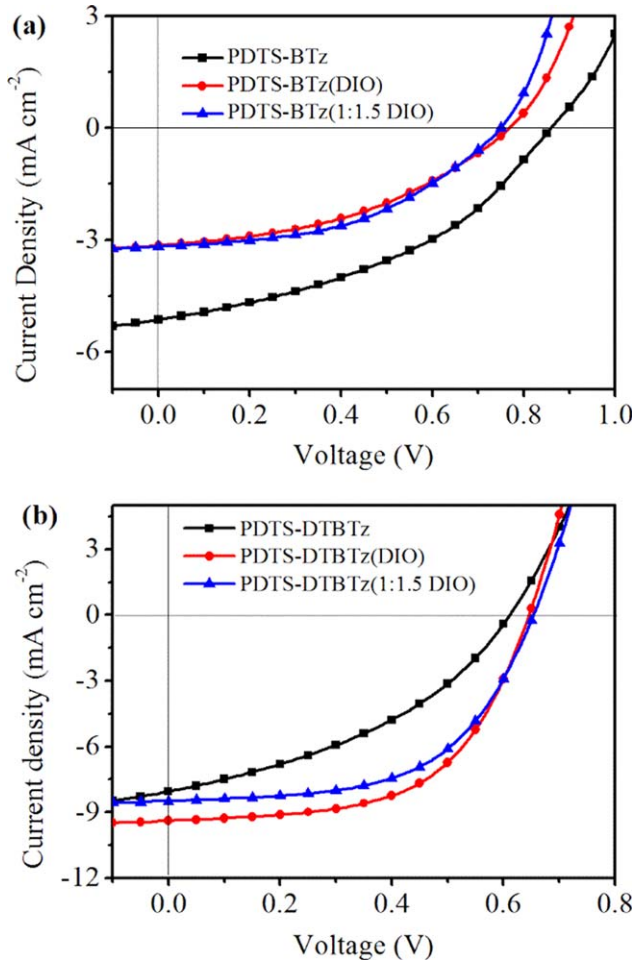

Figure 6. J-*V* curves of (a) PDTS-BTz:$PC_{71}BM$ or (b) PDTS-DTBTz:$PC_{71}BM$ based PSCs under AM 1.5 G illumination, 100 mW cm^{-2}. [Color figure can be viewed in the online issue, which is available at wileyonlinelibrary.com.]

Hole Mobility

Hole mobility of the two polymers:$PC_{71}BM$ (1 : 1) blend films was measured by the space-charge-limited-current (SCLC) method, as shown in Figure 5, the PDTS-DTBTz:$PC_{71}BM$ based device shows a hole mobility of 1.46×10^{-4} cm^2 V^{-1} S^{-1},

Table II. PSCs Performance with Device Configuration ITO/PEDOT:PSS/Polymer:$PC_{71}BM$/Ca/Al

Active layer	Ratio	DIO (%)	V_{oc} (V)	J_{sc} (mA cm^{-2})	*FF* (%)	*PCE* (%)
PDTS-BTz:$PC_{71}BM$	1 : 1	0	0.86	5.70	40.89	2.00
	1 : 1	0.5	0.77	3.14	41.89	1.01
	1 : 1.5	0.5	0.75	3.53	47.09	1.24
PDTS-DTBTz:$PC_{71}BM$	1 : 1	0	0.61	7.98	39.46	1.92
	1 : 1	0.5	0.65	9.39	57.06	3.46
	1 : 1.5	0.5	0.65	8.48	56.39	3.12

which is an order of magnitude higher than that (1.25×10^{-5} cm^2 V^{-1} S^{-1}) of PDTS-BTz:$PC_{71}BM$ based device, and this might due to the better planar structure and higher molecular weight[29] of PDTS-DTBTz. This could be a potential reason that PDTS-DTBTz:$PC_{71}BM$ based PSCs device exhibits larger J_{sc} and fill factor (FF) compared to PDTS-BTz:$PC_{71}BM$ based PSCs device.

Photovoltaic Performance and Morphology Characterization

Bulk heterojunction polymer solar cells were fabricated with a conventional device structure of ITO/PEDOT:PSS/polymer:$PC_{71}BM$ (~110 nm)/Ca/Al, and Figure 6 shows the *J-V* curves of PSCs under a simulated AM 1.5 G illumination of 100 mW cm^{-2}. $PC_{71}BM$ was used as the acceptor for its strong absorption in the visible region. To balance the absorption and the charge transporting network of the photoactive layer, the weight ratios of polymer and $PC_{71}BM$ were varied from 1.5 : 1 to 1 : 3. The other conditions, such as solvent, spin-coating speed, and additive, were also carefully optimized. The corresponding photovoltaic parameters of the devices are summarized in Table II.

The solvent additive of 1,8-diiodooctane (DIO) can affect the PSCs performance by morphology control. Without any solvent additives, the PDTS-BTz and PDTS-DTBTz based PSCs showed a similar *PCE* of 2.00% and 1.92%, respectively. When treated with DIO (0.5% v/v) additive, the photovoltaic properties of PDTS-DTBTz were greatly enhanced while PDTS-BTz sharply deteriorated. By increasing $PC_{71}BM$ weight ratio to 1 : 1.5, the device of PDTS-BTz still remain a relatively low *PCE*. However, the V_{oc} for the optimized PSCs based on PDTS-BTz:$PC_{71}BM$ blend was 0.86 V, which is 0.21 V higher than that (0.65 V) of the optimized PSCs based on PDTS-DTBTz. This could benefit from PDTS-BTz's lower lying HOMO energy level. The highest PCE of 3.46% for PDTS-DTBTz is obtained with a V_{oc} of 0.65 V, a J_{sc} of 9.39 mA cm^{-2}, and a FF of 57.06%, when the device was fabricated at donor–acceptor weight ratio of 1 : 1, containing 0.5% DIO as an additive, spin-cast from CB at a speed of 2000 rpm. After the introduction of thiophene, the J_{sc} and *FF* of PDTS-DTBTz increased while the V_{oc} decreased, compared with PDTS-BTz ($V_{oc} = 0.86$ V, $J_{sc} = 5.70$ mA cm^{-2}, $FF = 40.89\%$), as a result the *PCE* increased from 2.00% (without DIO) to 3.46%. The better photovoltaic performance of the thiophene-bridged copolymers could be ascribed to their higher hole mobility and better crystallinity.

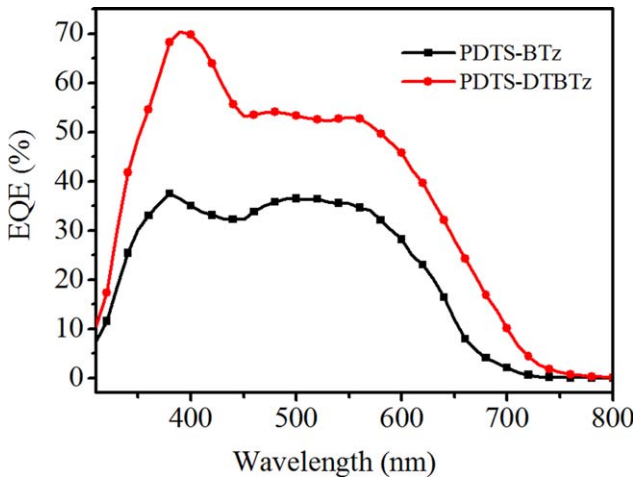

Figure 7. EQE curves of PSCs based on PDTS-BTz:$PC_{71}BM$ (1 : 1.5, w/w) or PDTS-DTBTz:$PC_{71}BM$ (1 : 1, w/w, 0.5% DIO). [Color figure can be viewed in the online issue, which is available at wileyonlinelibrary.com.]

Figure 7 demonstrates the external quantum efficiency (EQE) curves of the optimally fabricated PSCs based on these two copolymers. The PSCs devices exhibit broad response over 310–700 nm. The maximum EQE for the PDTS-BTz based device was 37% at 380 nm. In contrast, the PDTS-DTBTz-based device provided an EQE maximum of ca. 70% at 390 nm. The integral J_{sc} from EQE is 5.38 and 9.18 mA cm^{-2}, for PDTS-BTz and PDTS-DTBTz based devices, respectively, which are consistent with the measured J_{sc} from *J-V* curves.

The polymer/$PC_{71}BM$ blend film morphology with or without DIO were investigated by AFM. As shown in Figure 8, the blend films demonstrated different phase separation state with root-mean-square (RMS) roughness of 12.30 nm (e), 10.00 nm (f), 2.34 nm (g), and 2.12 nm (h). It can be observed from the phase images that PDTS-DTBTz/$PC_{71}BM$ film (d) formed nanoscale phase separation with appropriate domain sizes while the others showed some large scale phase separation. The much smaller RMS of PDTS-DTBTz [Figure 8(h)] could be ascribed to the application of thiophene as π-bridge units, which leads to a more flexible polymer main chain, and this indicate better miscibility between the polymer and $PC_{71}BM$. This could be another reason that

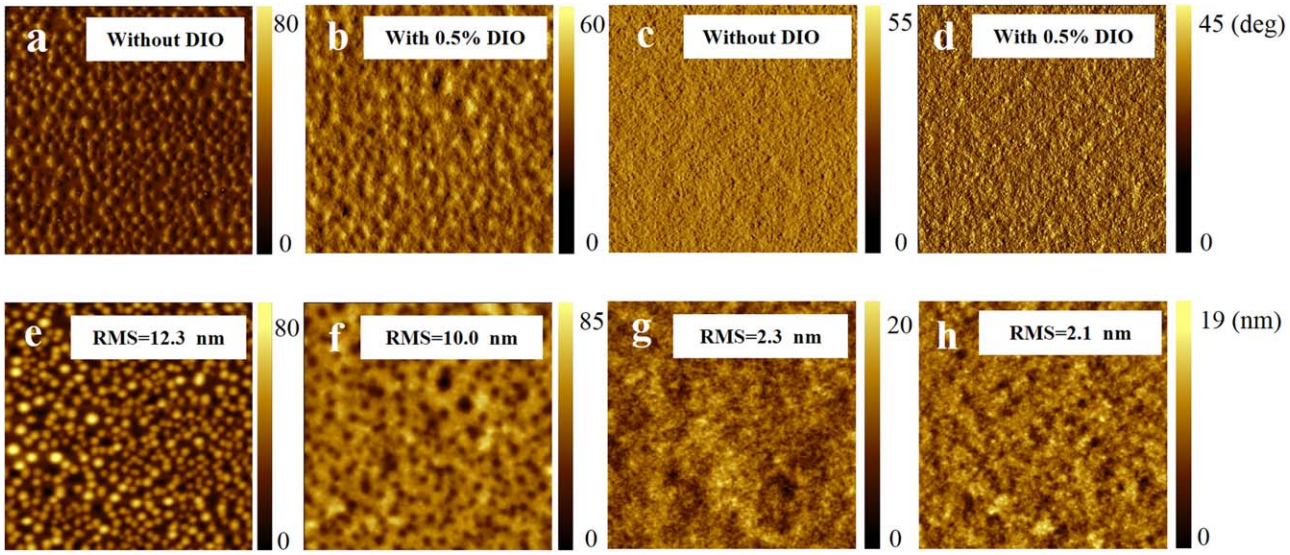

Figure 8. AFM phase (up) and height (down) images (5 μm × 5 μm) of PDTS-BTz:$PC_{71}BM$ =1 : 1 (a, e), PDTS-BTz:$PC_{71}BM$=1 : 1.5 (b, f), PDTS-DTBTz:$PC_{71}BM$=1 : 1 (c, g), and PDTS-DTBTz:$PC_{71}BM$ = 1 : 1 (d, h). [Color figure can be viewed in the online issue, which is available at wileyonlinelibrary.com.]

PDTS-DTBTz based PSCs devices exhibits larger J_{sc} and *FF* compared to PDTS-BTz.

CONCLUSIONS

In this work, two DTS and BTz backboned polymers were synthesized, and the thiophene π-bridge influence on the PSCs devices performances was studied. Both polymer show similar band gap, but polymer with thiophene π-bridge shows a little higher HOMO, more planar geometry, higher crystallinity, higher hole mobility, and better miscibility with fullerene. This is probably due to the insertion of thiophene π-bridge, and it could release the hindrance between donor and acceptor. Thus, it is much easier to get a polymer with higher molecular weight and better intermolecular π–π stacking. PDTS-BTz polymer based PSCs devices show higher V_{oc} due to the low-lying HOMO, but PDTS-DTBTz polymer do show enhanced overall PSCs performances. The present results indicate that thiophene π-bridge does contribute to the PSCs performances of the strong donor (dithienosilole) and weak acceptor (bithiazole) copolymer.

ACKNOWLEDGMENTS

The authors gratefully acknowledge financial support from the NSFC (21274134, 21274161, 21202181, 51173199, 61107090) and Shandong Province Postdoc Foundation (201301007).

REFERENCES

1. Kim, J. Y.; Lee, K.; Coates, N. E.; Moses, D.; Nguyen, T.-Q.; Dante, M.; Heeger, A. *J. Science* **2007**, *317*, 222.
2. Li, Y. *Accounts. Chem. Res.* **2012**, *45*, 723.
3. Cheng, Y.-J.; Yang, S.-H.; Hsu, C.-S. *Chem. Rev.* **2009**, *109*, 5868.
4. Chen, C.-C.; Dou, L.; Zhu, R.; Chung, C.-H.; Song, T.-B.; Zheng, Y. B.; Hawks, S.; Li, G.; Weiss, P. S.; Yang, Y. *ACS Nano* **2012**, *6*, 7185.
5. Scharber, M.; Sariciftci, N. *Prog. Polym. Sci.* **2013**, *38*, 1929.
6. You, J. B.; Dou, L. T.; Yoshimura, K.; Kato, T.; Ohya, K.; Moriarty, T.; Emery, K.; Chen, C. C.; Gao, J.; Li, G.; Yang, Y. *Nat. Commun.* **2013**, *4*, 10.
7. Liu, Y. H.; Zhao, J. B.; Li, Z. K.; Mu, C.; Ma, W.; Hu, H. W.; Jiang, K.; Lin, H. R.; Ade, H.; Yan, H. *Nat. Commun.* **2014**, *5*, 8.
8. Liu, C.; Yi, C.; Wang, K.; Yang, Y.; Bhatta, R. S.; Tsige, M.; Xiao, S.; Gong, X. *ACS Appl. Mater. Interfaces* **2015**, *7*, 4928.
9. Wang, E.; Ma, Z.; Zhang, Z.; Henriksson, P.; Inganäs, O.; Zhang, F.; Andersson, M. R. *Chem. Commun.* **2011**, *47*, 4908.
10. Zhou, E. J.; Cong, J. Z.; Hashimoto, K.; Tajima, K. *Macromolecules* **2013**, *46*, 763.
11. Han, L.; Chen, W.; Hu, T.; Ren, J.; Qiu, M.; Zhou, Y.; Zhu, D.; Wang, N.; Sun, M.; Yang, R. *ACS Macro. Lett.* **2015**, *4*, 361.
12. Zhang, Z. G.; Wang, J. Z. *J. Mater. Chem.* **2012**, *22*, 4178.
13. Hong, Y. R.; Ng, J. Y.; Wong, H. K.; Moh, L. C. H.; Yip, Y. J.; Chen, Z. K.; Norsten, T. B. *Sol. Energy. Mater. Sol. C* **2012**, *102*, 58.
14. Dang, D. F.; Xiao, M. J.; Zhou, P.; Shi, J. W.; Tao, Q.; Tan, H.; Wang, Y. F.; Bao, X. C.; Liu, Y.; Wang, E. G.; Yang, R. Q.; Zhu, W. G. *Org. Electron.* **2014**, *15*, 2876.
15. Wang, X. C.; Sun, Y. P.; Chen, S.; Guo, X.; Zhang, M. J.; Li, X. Y.; Li, Y. F.; Wang, H. Q. *Macromolecules* **2013**, *46*, 2521.
16. Gu, C. T.; Xiao, M. J.; Bao, X. C.; Han, L. L.; Zhu, D. Q.; Wang, N.; Wen, S. G.; Zhu, W. G.; Yang, R. Q. *Polym. Chem.* **2014**, *5*, 6551.
17. Guo, X.; Zhang, M. J.; Huo, L. J.; Xu, F.; Wu, Y.; Hou, J. H. *J. Mater. Chem.* **2012**, *22*, 21024.

18. Svensson, M.; Zhang, F. L.; Veenstra, S. C.; Verhees, W. J. H.; Hummelen, J. C.; Kroon, J. M.; Inganas, O.; Andersson, M. R. *Adv. Mater.* **2003**, *15*, 988.
19. Hou, J. H.; Chen, H. Y.; Zhang, S. Q.; Li, G.; Yang, Y. *J. Am. Chem. Soc.* **2008**, *130*, 16144.
20. Huo, L. J.; Chen, H. Y.; Hou, J. H.; Chen, T. L.; Yang, Y. *Chem. Commun.* **2009**, *37*, 5570.
21. Medlej, H.; Awada, H.; Mamatimin, A. B.; Wantz, G.; Bousquet, A.; Grelet, E.; Hariri, K.; Hamieh, T.; Hiorns, R. C.; Dagron-Lartigau, C. *Euro. Polym. J.* **2013**, *49*, 4176.
22. Chu, T. Y.; Lu, J. P.; Beaupre, S.; Zhang, Y. G.; Pouliot, J. R.; Wakim, S.; Zhou, J. Y.; Leclerc, M.; Li, Z.; Ding, J. F.; Tao, Y. *J. Am. Chem. Soc.* **2011**, *133*, 4250.
23. Huo, L. J.; Hou, J. H.; Chen, H. Y.; Zhang, S. Q.; Jiang, Y.; Chen, T. L.; Yang, Y. *Macromolecules* **2009**, *42*, 6564.
24. Lee, S. K.; Lee, J.; Lee, H. Y.; Yoon, S. C.; Kim, J. R.; Kim, K. N.; Kim, H. J.; Shin, W. S.; Moon, S.-J. *J. Nanosci. Nanotechno.* **2011**, *11*, 4279.
25. Min, J.; Zhang, Z. G.; Zhang, S. Y.; Zhang, M. J.; Zhang, J.; Li, Y. F. *Macromolecules* **2011**, *44*, 7632.
26. Zhang, M. J.; Fan, H. J.; Guo, X.; He, Y. J.; Zhang, Z. G.; Min, J.; Zhang, J.; Zhao, G. J.; Zhan, X. W.; Li, Y. F. *Macromolecules* **2010**, *43*, 5706.
27. Zhang, M. J.; Guo, X.; Li, Y. F. *Adv. Energy Mater.* **2011**, *1*, 557.
28. Zhang, M. J.; Guo, X.; Li, Y. F. *Macromolecules* **2011**, *44*, 8798.
29. Huang, J. H.; Chen, F. C.; Chen, C. L.; Huang, A. T.; Hsiao, Y. S.; Teng, C. M.; Yen, F. W.; Chen, P. L.; Chu, C. W. *Org. Electron.* **2011**, *12*, 1755.
30. Huang, J. H.; Huang, A. T.; Hsu, C. Y.; Lin, J. T.; Chu, C. W. *Sol. Energy. Mater. Sol. C* **2012**, *98*, 300.
31. Huang, J. H.; Teng, C. M.; Hsiao, Y. S.; Yen, F. W.; Chen, P. L.; Chang, F. C.; Chu, C. W. *J. Phys. Chem. C* **2011**, *115*, 2398.
32. Wang, J. X.; Xiao, M. J.; Chen, W. C.; Qiu, M.; Du, Z. K.; Zhu, W. G.; Wen, S. G.; Wang, N.; Yang, R. Q. *Macromolecules* **2014**, *47*, 7823.
33. Kline, R. J.; McGehee, M. D.; Toney, M. F. *Nat. Mater.* **2006**, *5*, 222.
34. Kim, Y.; Cook, S.; Tuladhar, S. M.; Choulis, S. A.; Nelson, J.; Durrant, J. R.; Bradley, D. D. C.; Giles, M.; McCulloch, I.; Ha, C. S.; Ree, M. *Nat. Mater.* **2006**, *5*, 197.